Journal of Catalysis 299 (2013) 1–9

Contents lists available at SciVerse ScienceDirect

Journal of Catalysis

journal homepage: www.elsevier.com/locate/jcat

A feasible approach to the synthesis of nickel phosphide for hydrodesulfurization

Qingxin Guan, Xun Cheng, Rongguan Li, Wei Li *

Key Laboratory of Advanced Energy Materials Chemistry (Ministry of Education), College of Chemistry, Nankai University, Tianjin 300071, China

ARTICLE INFO

Article history:
Received 30 July 2012
Revised 2 November 2012
Accepted 7 November 2012

Keywords:
Desulfurization
Hydrogen
Metal phosphide
Nickel
Phosphate

ABSTRACT

In this paper, we propose a simple and feasible method for synthesizing bulk and supported nickel phosphides from oxide precursors. The new approach uses a low hydrogen flow speed and is not affected by the heating rate. The results indicate that Ni_2P can be synthesized at 600 °C from its oxide precursors with a mole ratio of Ni/P = 2/1. The hydrodesulfurization activity results indicate that the direct-reduction method shows excellent performance in the synthesis of supported catalysts.

1. Introduction

Noble metals (e.g., Pt, Pd, Rh, Au) are very useful in many scientific fields because of their excellent performance. However, the low availability of noble metals severely restricts their wider application. Interstitial compounds have attracted considerable attention in recent decades and have emerged in more and more areas (e.g., dye-sensitized solar cells, fuel cells, catalysis) as alternative materials to noble metals [1,2]. Among the various types of interstitial compounds, metal phosphides have definitely emerged as superstars because of their unexpected properties in catalysis, magnetic applications, and applications in telecommunications, electronic and optoelectronic devices, lithium batteries, and solar cells [1,3]. However, the difficulty of preparing metal phosphides inhibits their use in large-scale applications.

Metal phosphides were reported as early as the 1930s [4], and their synthesis and applications underwent tremendous development in the following decades. A variety of methods for synthesizing metal phosphides have been reported [3,5–18]. Generally, the solvothermal method is not feasible for the deposition of metal phosphides on supports. The temperature-programmed reduction (TPR) method has proved to be an effective and general way to prepare bulk and supported metal phosphides [5]. However, the synthesis requires strict temperature-programmed steps and relatively high temperatures. The conversion of oxide precursors to phosphides by H_2 reduction is neither thermodynamically nor kinetically favorable [12]. Hence, the forward reaction has to be aided by high temperature and low water vapor pressure [19]. Thus, Ni_2P can only be obtained with a low heating rate, excess phosphorus, and a high H_2 flow speed, as has been recognized by most researchers in recent decades. However, based on the above analysis, we could not reach the conclusion that the strict temperature-programmed steps are indispensable. In our recent studies, we performed a new examination of the reduction of metal phosphate precursors and obtained some unexpected results.

2. Experimental methods

Siliceous MCM-41 was purchased from Tianjin Chemist Scientific Ltd., China. It had a specific surface area of 956 $m^2\ g^{-1}$, a pore volume of 1.1 $cm^3\ g^{-1}$, and a BJH average pore size of 3.32 nm. Dibenzothiophene (DBT) was of analytical pure grade and purchased from Alfa Aesar. Other reagents were analytical pure grade and purchased from Tianjin Guangfu Fine Chemical Research Institute, China.

2.1. Synthesis of bulk and supported nickel phosphides

The synthesis of nickel phosphide involves two main steps: (1) the oxidic precursor is obtained by coimpregnation with an aqueous solution of diammonium hydrogen phosphate ($(NH_4)_2HPO_4$) and nickel(II) nitrate ($Ni(NO_3)_2{\cdot}6H_2O$), followed by drying and calcination; (2) the precursor is converted to nickel phosphide in flowing H_2. In a typical experiment, bulk nickel phosphide was obtained as follows. Initially, 14.84 g of $Ni(NO_3)_2{\cdot}6H_2O$ and 3.35 g of $(NH_4)_2HPO_4$ were dissolved in 27 mL of deionized water and stirred for 1 h. Then, the slurry was evaporated at

* Corresponding author. Fax: +86 22 23508662.
E-mail address: weili@nankai.edu.cn (W. Li).

0021-9517/$ - see front matter © 2012 Elsevier Inc. All rights reserved.
http://dx.doi.org/10.1016/j.jcat.2012.11.008

120 °C for 3 h and calcined at 500 °C for 2 h to obtain the precursor. Subsequently, 0.6 g of precursor and 10 mL of quartz sand were loaded into the quartz tube reactor (as a preliminary heating zone). The precursor materials were then reduced to phosphides in H_2 flow (60 mL min^{-1}) at 600 °C for 1 h. Finally, the product was cooled to ambient temperature under flowing H_2 and was passivated for 1 h under flowing 1% O_2/N_2. Similarly to the synthesis of bulk nickel phosphide, supported nickel phosphide was prepared by reducing the supported oxidic precursor in flowing H_2.

For comparison, bulk and MCM-41-supported Ni_2P were also successfully prepared using the TPR method [20]. The temperature program was as follows. The flow rate of H_2 in the whole procedure was 250 mL min^{-1}. A heating rate of 5 °C min^{-1} was used from room temperature to 400 °C, and temperature was maintained at 400 °C for 1 h. Then, a heating rate of 2 °C min^{-1} was used from 400 to 600 °C, and temperature was maintained at 600 °C for 3 h. Subsequently, the product was cooled to ambient temperature under flowing H_2 and was passivated for 1 h under flowing 1% O_2/N_2.

2.2. Characterization

Powder X-ray diffraction (XRD) was performed on a Bruker D8 focus diffractometer with Cu Kα radiation at 40 kV and 40 mA. The compositions of the samples were measured using atomic absorption spectrophotometry (AAS). The transmission electron microscopy (TEM) images were acquired using a Philips Tecnai G^2 F-20 field emission gun transmission electron microscope. Scanning electron microscopy (SEM) images were acquired using a Tescan Vega3 SBH scanning electron microscope. Nitrogen adsorption was measured with a BEL-Mini adsorption analyzer. The CO chemisorption was performed with Micromeritics Chemisorb 2750 gas-adsorption equipment. The sample was loaded into a quartz reactor and pretreated in 10% H_2/Ar at 450 °C for 3 h. After cooling in He, pulses of 10% CO/He in a He carrier (25 mL (NTP) min^{-1}) were injected at 30 °C through a loop tube. The H_2 TPR of samples was performed with Micromeritics Chemisorb 2750 gas-adsorption equipment. The sample was loaded into a quartz reactor and pretreated in He at 600 °C for 3 h. After cooling in He, the sample was reduced using 10% H_2/Ar as the reducing gas at a heating rate of 10 °C min^{-1} up to 950 °C. The gas flow rate was 25 mL min^{-1}. X-ray photoelectron spectra (XPS) were recorded using a Kratos Axis Ultra DLD spectrometer employing a monochromated Al Kα X-ray source ($h\nu$ = 1486.6 eV), hybrid (magnetic/electrostatic) optics, and a multichannel plate and delay line detector. All XPS spectra were recorded using an aperture slot of 300 × 700 μm, survey spectra were recorded with a pass energy of 80 eV, and high-resolution spectra with a pass energy of 40 eV. To subtract the surface charging effect, the C1*s* peak has been fixed at a binding energy of 284.6 eV.

2.3. Catalytic activity test

The HDS catalytic activities were evaluated using 3000 ppm DBT in decalin. The HDS reaction was carried out in a fixed-bed microreactor. The catalyst was pelleted, crushed, and sieved with 20–40 mesh. One gram of the catalyst was diluted with SiO_2 to a volume of 5.0 mL in the reactor. Prior to the reaction, catalysts were pretreated in situ with flowing H_2 (60 mL min^{-1}) for 3 h. The testing conditions for the HDS reaction were 3 MPa, weight hourly space velocity (WHSV) = 6 h^{-1}, and H_2/oil = 720. Liquid products were collected every hour after a stabilization period of 6 h. Both feed and products were analyzed with a FuLi 9790 gas chromatograph equipped with a flame ionization detector and an OV-101 column. The DBT conversion and turnover frequency (TOF) were used to evaluate the HDS activity. The TOF was calculated using the equation

$$\mathrm{TOF} = \frac{F_{Ao}}{W}\frac{X_A}{\mathrm{CO}_{\mathrm{uptake}}}, \quad (1)$$

where F_{Ao} is the molar rate of reactant fed into the reactor (μmol s^{-1}), W is the catalyst weight (g), CO_{uptake} is the uptake of chemisorbed CO (μmol g^{-1}), and X_A is the reactant conversion (%).

3. Results and discussion

3.1. Synthesis of bulk and supported nickel phosphides

The oxide precursor of $4NiO{\cdot}P_2O_5$ was obtained by calcination of nickel(II) phosphate at 600 °C. As shown in Fig. 1, the H_2 TPR results indicate that the oxide precursor of $4NiO{\cdot}P_2O_5$ is not a simple mixture of NiO and P_2O_5, which is an amorphous compound, and no diffraction peaks were detected in the XRD patterns. The high temperature in the H_2 TPR experiment also indicated that this reaction is thermodynamically unfavorable and a high temperature is required. However, these data do not demonstrate that a low heating rate and high H_2 flow speed are indispensable.

In this paper, a simple improvement in the reaction process completely broke the requirement for the strict temperature-programmed steps, namely the use of a preheating zone and low H_2 flow speed. To confirm the method, many experiments were performed using Ni_2P as a model compound. As shown in Fig. 2, the synthesis of Ni_2P was not affected by heating rates, and Ni_2P could

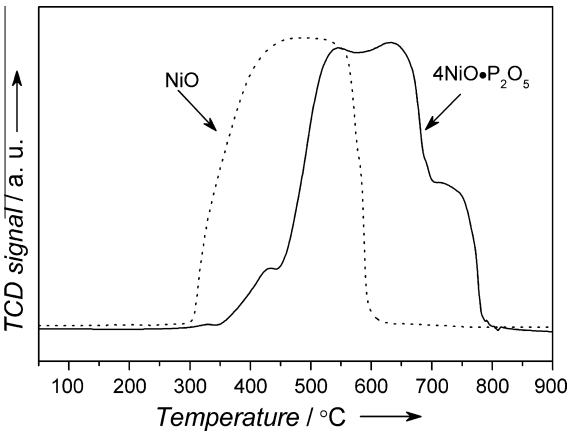

Fig. 1. The H_2 TPR patterns of different oxide precursors at a heating rate of 10 °C min^{-1}.

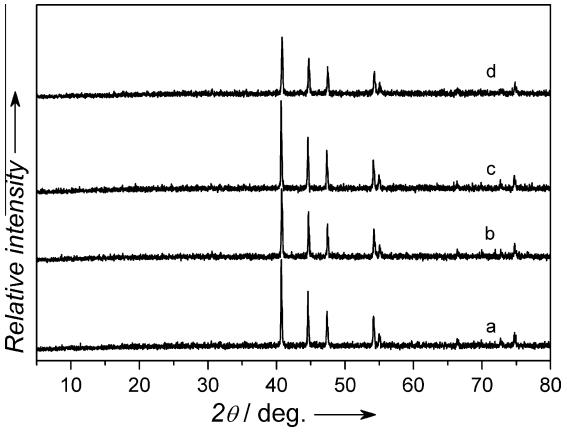

Fig. 2. The XRD patterns of bulk Ni_2P prepared from oxide precursors (in a mole ratio of Ni/P = 2/1) using different heating rates: (a) TPR method steps, (b) 5 °C min^{-1}, (c) 20 °C min^{-1}, (d) was reduced directly at 600 °C.

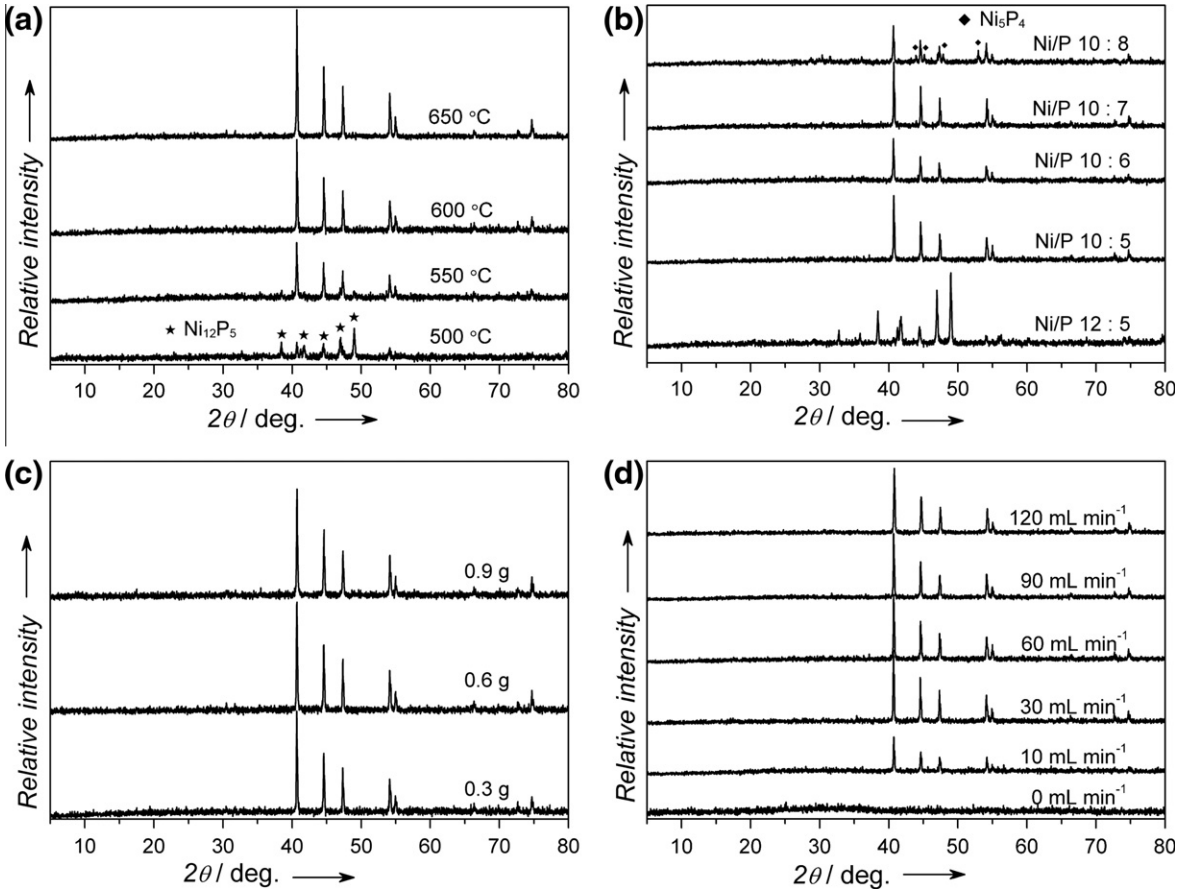

Fig. 3. The XRD patterns of bulk nickel phosphides prepared from oxide precursors in the same quartz tubes: (a) different calcination temperatures, (b) different mole ratios of Ni/P, (c) different loadings, and (d) different H_2 flow speeds.

be synthesized at different heating rates; it was even reduced directly at 600 °C for 1 h. Furthermore, as shown in Fig. 3, the impacts of the calcination temperature, mole ratios of Ni/P, loadings, and H_2 flow speed were studied in the same quartz tube. The results indicate that Ni_2P can be synthesized at 600 °C from the oxide precursors with a mole ratio of Ni/P = 2/1, and the synthesis conditions (e.g., loadings and H_2 flow speed) were very broad. The calcination temperature and mole ratio of Ni/P are the key factors in the synthesis. Decreasing the mole ratio of Ni/P leads to the generation of phosphorus-rich products (e.g., Ni_5P_4). Decreasing the calcination temperature leads to the generation of $Ni_{12}P_5$ from oxide precursors at a mole ratio of Ni/P = 2/1 (Fig. 3a). According to density functional theory, the larger the number of *d* orbitals of Ni that are not bonded to *p* orbitals of P, the less stable will be the surface, because the dangling bonds formed by unbonded *d* orbitals increase the surface energy [21].

As shown in Fig. 4, the compositions of terminated layers of Ni_2P and $Ni_{12}P_5$ were Ni_3P and Ni_4P_5, respectively. The Ni_4P_5 structure has a lower surface energy than the Ni_3P structure, which is more stable under the same conditions. As shown in Table 1 [22], Ni_2P has a lower atomic density than $Ni_{12}P_5$, which is more stable at higher temperatures in the mole ratio Ni/P = 2/1. Hence, the appearance of $Ni_{12}P_5$ at low temperatures might be determined by its low surface energy, while the appearance of Ni_2P at high temperatures might be determined by its lower atomic density. To further study the surfaces of bulk Ni_2P and $Ni_{12}P_5$ samples, the XPS technique was employed. The results show that the superficial atomic ratios of Ni/P are 0.41 and 0.57 for Ni_2P and $Ni_{12}P_5$, respectively. Fig. 5 shows the Ni2*p* and P2*p* core level spectra of bulk Ni_2P and $Ni_{12}P_5$. The Ni2*p* core level spectrum of Ni_2P involves

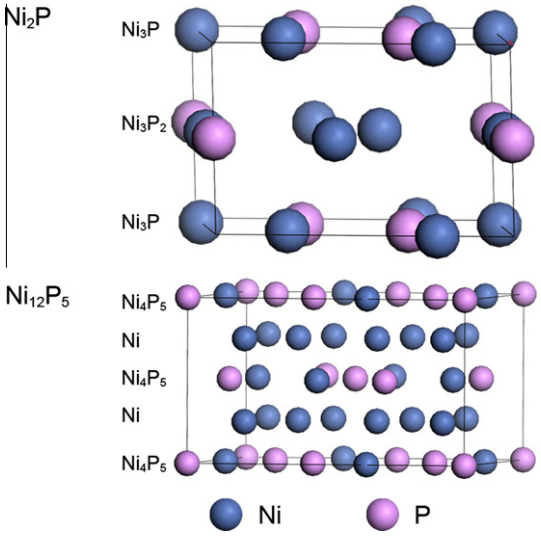

Fig. 4. The structures of Ni_2P and $Ni_{12}P_5$ phases show the alternation of differently terminated layers.

two peaks (Fig. 5a). The first one is assigned to $Ni^{\delta+}$ of Ni_2P and centered at 853.1 eV, and the second one is at 856.4 eV, corresponding to Ni^{2+} ions interacting possibly with phosphate ions as a consequence of a superficial passivation [6]. Meanwhile, the P2*p* binding energy of Ni_2P was observed at 129.7 eV for $P^{\delta-}$ of Ni_2P and 133.7 eV for surface nickel phosphate species [6], due to the

Table 1
The lattice parameters of Ni_2P and $Ni_{12}P_5$.

Metal phosphides	a (Å)	b (Å)	c (Å)	α (°)	β (°)	γ (°)	Atom number	Unit cell volume (Å^3)	Atomic density (Å^{-3})
Ni_2P	5.859	5.859	3.382	90	90	120	9	100.54	8.952×10^{-2}
$Ni_{12}P_5$	8.646	8.646	5.07	90	90	90	34	379	8.971×10^{-2}

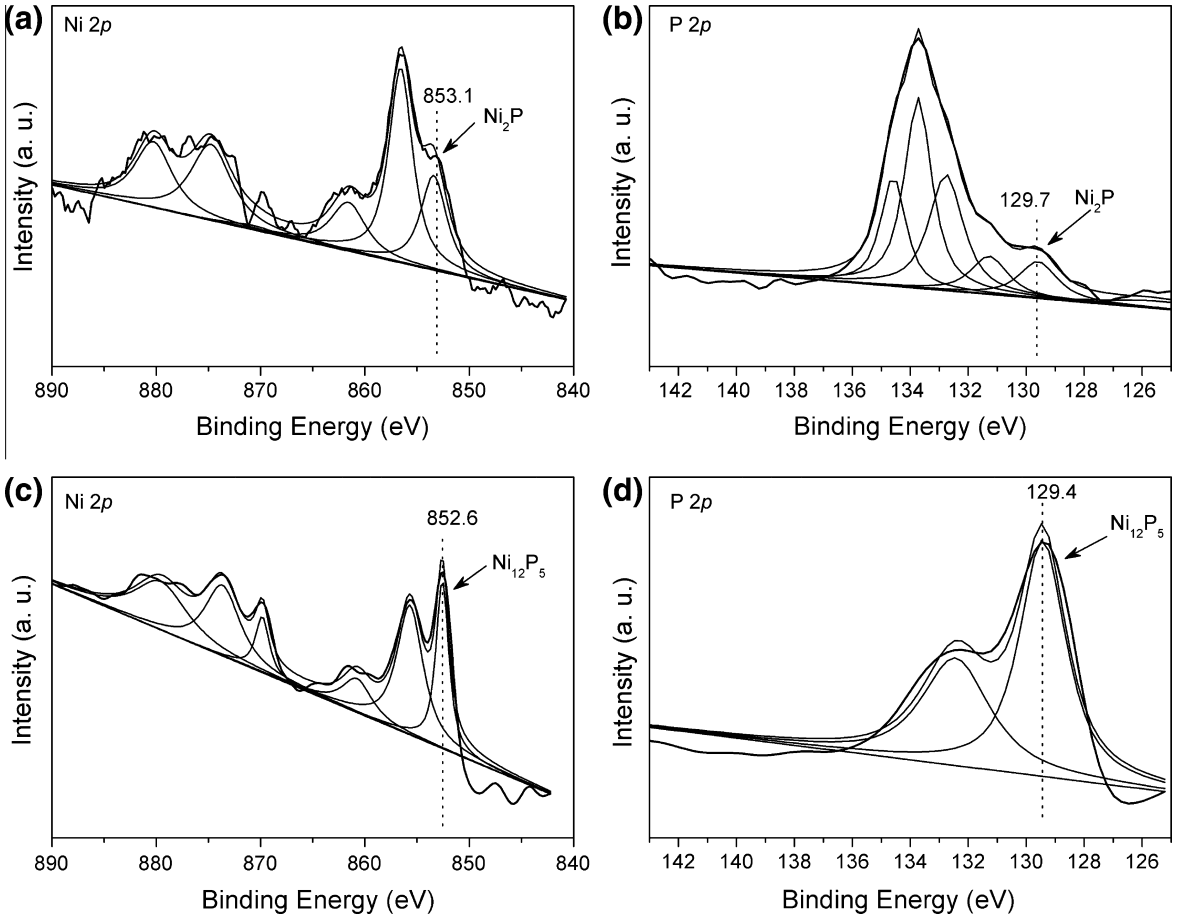

Fig. 5. The XPS spectra of bulk Ni_2P and $Ni_{12}P_5$ samples: (a) Ni2*p* core level spectra of Ni_2P, (b) P2*p* core level spectra of Ni_2P, (c) Ni2*p* core level spectra of $Ni_{12}P_5$, and (d) P2*p* core level spectra of $Ni_{12}P_5$.

superficial oxidation of Ni_2P. Similarly, the binding energy assigned to $Ni^{\delta+}$ and $P^{\delta-}$ of $Ni_{12}P_5$ is observed at 852.6 and 129.4 eV. Interestingly, the peak of Ni^{2+} in the Ni_2P sample is significantly higher than that of $Ni_{12}P_5$, which might be caused by its lower atomic density. As shown in Table 1, Ni_2P has a lower atomic density than $Ni_{12}P_5$, and oxygen atoms more easily penetrate the interior of crystals in the process of superficial passivation. Hence, Ni_2P shows a higher Ni^{2+} peak than $Ni_{12}P_5$ in the Ni2*p* core level spectrum. As shown in Fig. 5c, the $Ni_{12}P_5$ sample shows slightly lower binding energy than Ni_2P, which might be affected by its lower content of nickel phosphate.

In considering the parameters, the calcination time is also an important factor. To exclude the effects of the heating rate, H_2 was pumped in and, simultaneously, the time was recorded after the reactor temperature reached the set value. Fig. 6 shows the XRD patterns of bulk nickel phosphides prepared from oxide precursors with different calcination times. The results clearly show that the product changes from $Ni_{12}P_5$ to Ni_2P with time and that Ni_2P can be synthesized in 60 min. This conclusion is also confirmed by SEM images, which show visible changes with increasing calcination time (Fig. 7).

To analyze further the composition of the bulk products, bulk Ni_2P samples that were synthesized in 60, 120, and 180 min were analyzed using an atomic absorption spectrophotometer. The results indicate that the nickel content of the three samples is 79.15, 79.14, and 79.17 wt%, respectively, which are close to the calculated value (79.10 wt%). Thus, the bulk sample that was synthesized in 60 min is the pure Ni_2P phase. As shown in Fig. 8, Ni_2P samples supported on MCM-41 with different loadings were prepared by impregnation. The XRD results indicate that the typical diffraction peaks of Ni_2P appeared in 30 wt% Ni_2P/MCM-41. The XRD peaks of Ni_2P were not detected at the loadings of 10 and 20 wt%, which might be because the supported Ni_2P nanoparticles were tiny and below the detection limit. For comparison, the XRD pattern of 30 wt% Ni_2P/MCM-41 prepared using the TPR method is given in Fig. 8, which shows a result similar to those prepared using the direct-reduction method. This method is simple and does not require temperature-programmed steps; accordingly, we named it the direct-reduction (DR) method.

For comparison, the impact of mole ratios of Ni/P was also studied using the TPR method. Fig. 9 shows the XRD patterns of bulk nickel phosphide prepared using the TPR method at 600 °C from

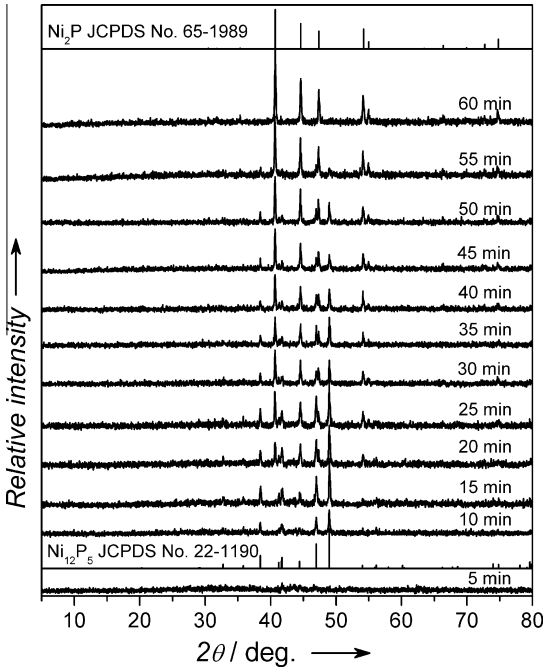

Fig. 6. The XRD patterns of bulk nickel phosphides prepared from oxide precursors with different calcination times at a H_2 flow speed of 60 mL min^{-1}.

oxide precursors with different mole ratios of Ni/P. It is seen that the diffraction peaks of $Ni_{12}P_5$ gradually disappear with decreasing mole ratios of Ni/P, and that Ni_2P was synthesized with a mole ratio of Ni/P = 10/8. The crystal size of bulk Ni_2P was calculated with the Scherrer formula, and the calculated result was compared with the TEM observed result. Table S1 gives the Scherrer particle sizes of bulk Ni_2P prepared using different methods. The bulk nickel phosphides prepared using the DR and TPR methods have similar

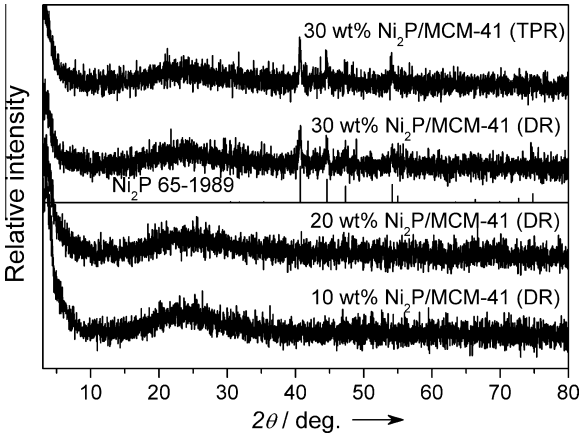

Fig. 8. The XRD patterns of Ni_2P supported on MCM-41 with different loadings.

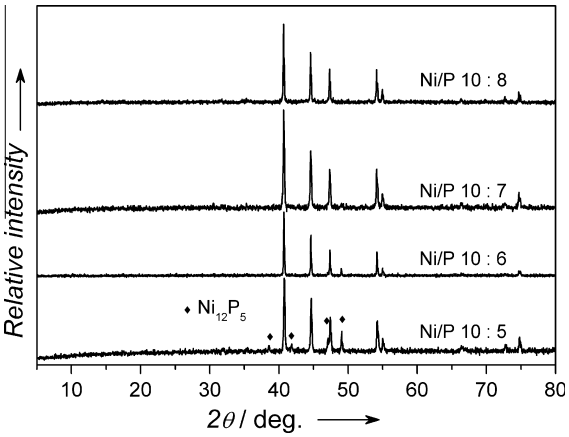

Fig. 9. The XRD patterns of bulk nickel phosphide prepared using the TPR method at 600 °C from oxide precursors with different mole ratios of Ni/P.

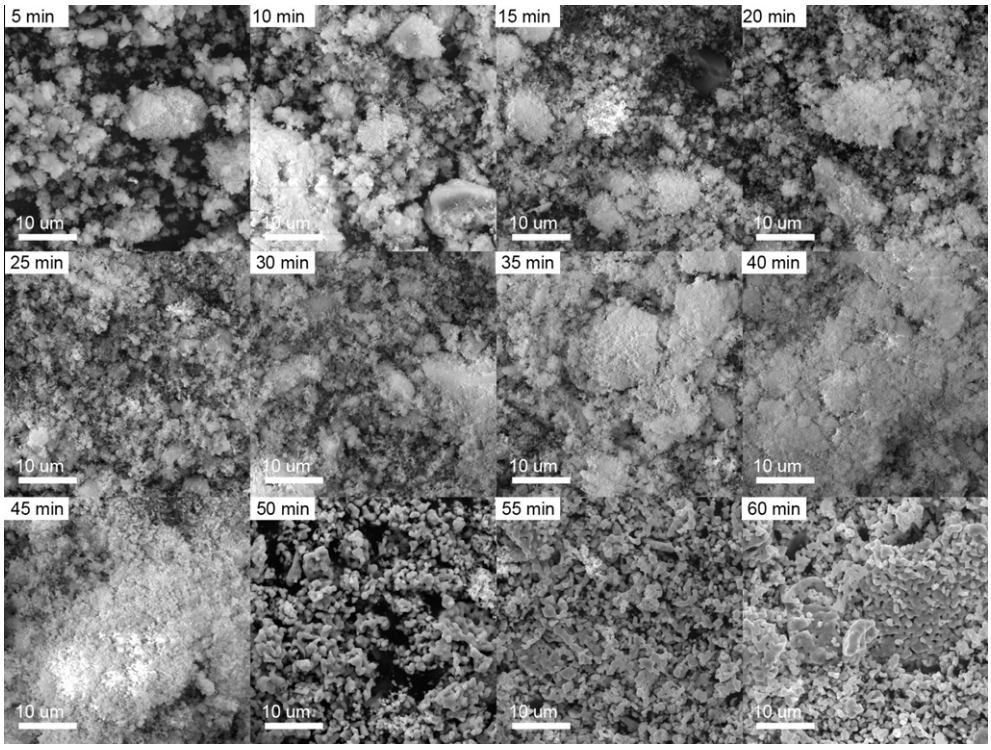

Fig. 7. The SEM images of samples prepared from oxide precursors with different calcination times at a H_2 flow speed of 60 mL min^{-1}.

Table 2
The optimal synthetic conditions for the preparation of different metal phosphide synthesized from metal phosphate precursors using the direct-reduction method.

Metal phosphide[a]	Mole ratios	Temperature (°C)	H_2 (mL min^{-1})	Reduction time (h)
$Ni_{12}P_5$	Ni:P = 12:5	600	60	1
Ni_2P	Ni:P = 2:1	600	60	1
CoP	Co:P = 1:1	600	60	1
Co_2P	Co:P = 2:1	600	60	1
MoP	Mo:P = 1:1.1	650	60	3
WP	W:P = 1:1.1	650	60	3
MoNiP	Ni:Mo:P = 1:1:1.1	650	60	3

[a] The loading of different precursors is 0.6 g in all experiments.

Scherrer particle sizes of about 50 nm. Fig. S1 gives the TEM images of bulk Ni_2P prepared using the DR and TPR methods. The observed particle size of bulk Ni_2P prepared using the DR and TPR methods is about 50–100 nm, which is larger than the calculated Scherrer particle size. The difference in the above results might be caused by the inaccuracy of the Scherrer formula.

To illustrate the versatility of this synthetic method, different metal phosphides were synthesized. Table 2 gives the optimal synthetic conditions for the preparation of different metal phosphides using the DR method. For MoP, WP, and MoNiP, excess phosphorus is required because the high temperature and long calcination time cause a small amount of phosphorus loss. Fig. 10 shows the XRD patterns and SEM images of different metal phosphides synthesized using the DR method. The results show that bulk $Ni_{12}P_5$, Co_2P, CoP, MoP, WP, and MoNiP could be synthesized using the DR method, thus indicating that those metal phosphides synthesized using the TPR method can also be synthesized by the DR method.

3.2. HDS activity

In our previous studies, the Ni_2P/MCM-41 catalyst could be synthesized at lower temperatures using the decomposition of hypophosphites [13,14]. In this paper, a series of Ni_2P/MCM-41 catalysts were synthesized at 600 °C from metal phosphate precursors using the DR method. Hence, for comparison, Ni_2P/MCM-41 catalysts prepared by the TPR method were synthesized and tested under the same conditions. To investigate the properties and catalytic activities, Ni_2P/MCM-41 catalysts prepared by different methods were characterized and tested by TEM, nitrogen adsorption, CO chemisorption, and HDS. The DBT conversion and TOF were used to evaluate the HDS activity [23]. The TOF was calculated using Eq. (1). Irreversible CO uptake measurements were used to titrate the surface metal atoms and to provide an estimate of the active sites on the catalysts [24]. All of the catalytic activities were tested using the ninth-hour liquid products after a stabilization period.

As shown in Fig. 11, TEM images of the Ni_2P/MCM-41 prepared by the DR method show fairly uniform nanoparticles, which indicates good dispersion on the MCM-41 support. The TEM images (Fig. 11a and b) also show that the particle size of Ni_2P clearly

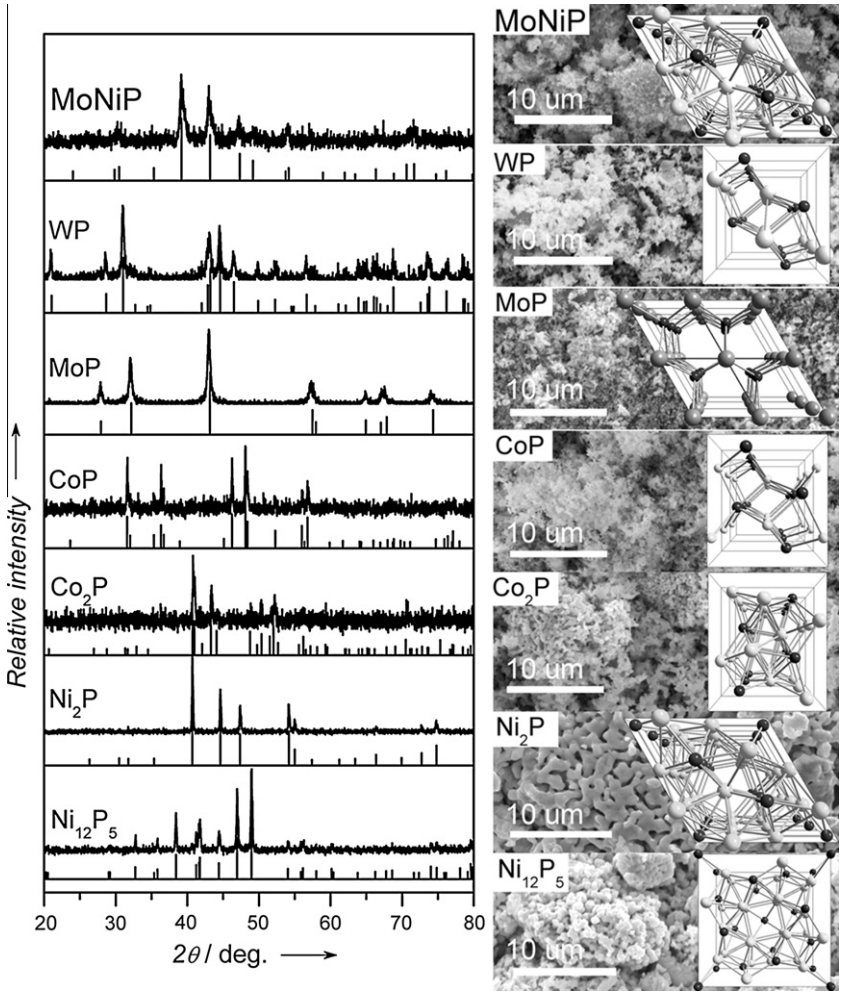

Fig. 10. The XRD patterns and SEM images of different metal phosphides synthesized using the direct-reduction method.

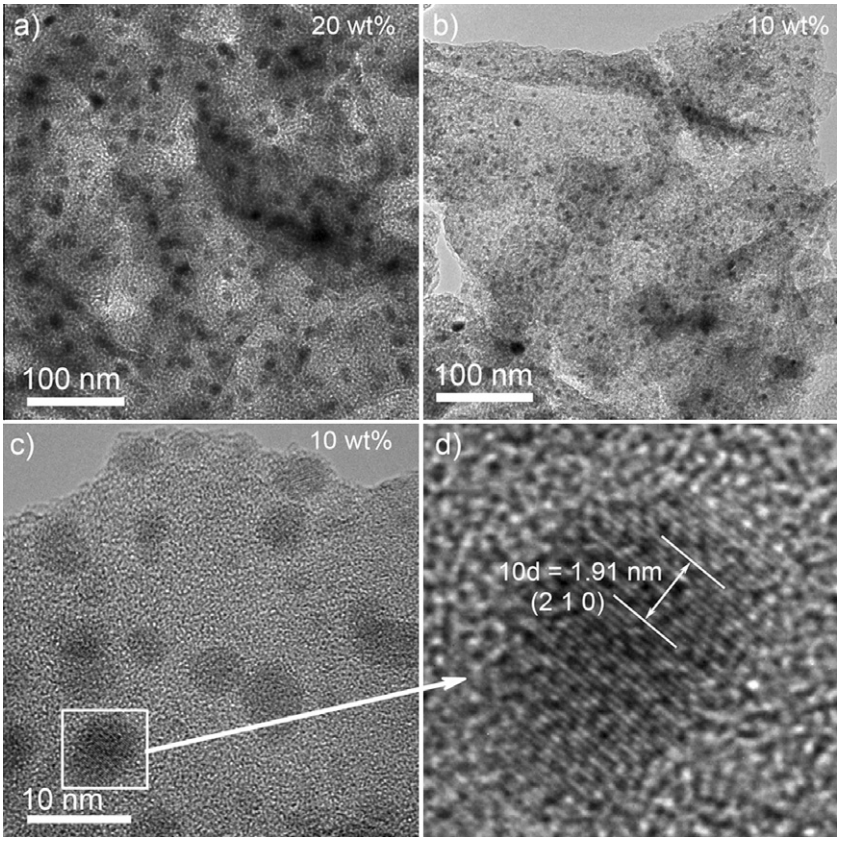

Fig. 11. The TEM images of Ni_2P/MCM-41 with different loadings.

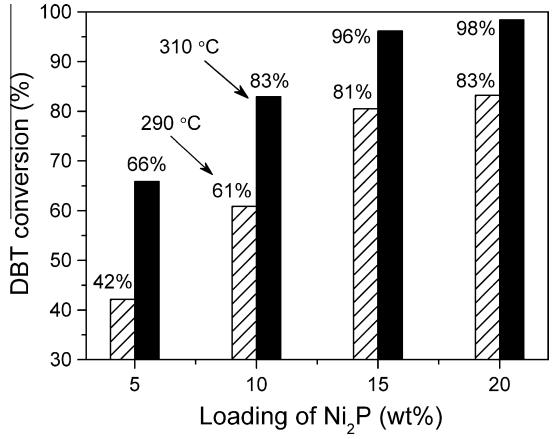

Fig. 12. The catalytic activities of Ni_2P/MCM-41 with different loadings (testing conditions: 3 MPa, WHSV = 6 h^{-1}, H_2/oil = 720).

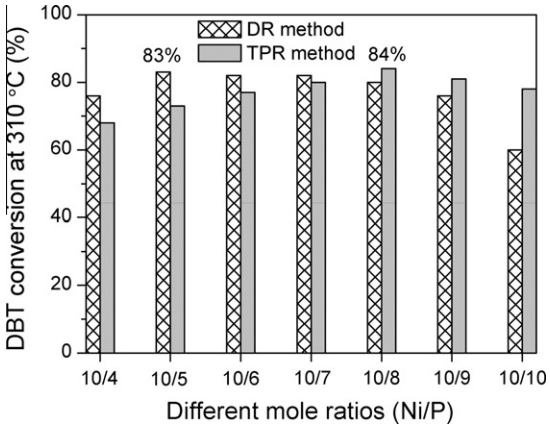

Fig. 13. The catalytic activities of 10 wt% Ni_2P/MCM-41 prepared from the precursors with different mole ratios of Ni/P (testing conditions: 3 MPa, 310 °C, WHSV = 6 h^{-1}, H_2/oil = 720).

decreased with decreasing loading. A magnified high-resolution TEM image of a selected frame from Fig. 11c given in Fig. 11d yields *d*-spacing values of 0.191 nm for the (2 1 0) crystallographic planes of Ni_2P, which is in good agreement with the calculated value. This indicates the formation and good dispersion of nanocrystalline Ni_2P on the MCM-41 support.

Fig. 12 gives the catalytic activities of Ni_2P/MCM-41 with different loadings. The result shows that the catalytic activities of Ni_2P/MCM-41 both at 290 and at 310 °C gradually increased with increasing Ni_2P loadings. This result is generally accepted; for Ni_2P/MCM-41, higher temperature favors HDS of DBT. To compare the catalytic activities of Ni_2P/MCM-41 catalysts prepared using the DR and TPR methods, a series of 10 wt% Ni_2P/MCM-41 samples were prepared from the precursors with different mole ratios of Ni/P. Subsequently, these catalysts were tested in HDS of DBT at 310 °C. Fig. 13 shows the catalytic activities at 310 °C of 10 wt% Ni_2P/MCM-41 prepared from precursors with different mole ratios of Ni/P. The results indicate that the highest DBT conversion at 310 °C of 10 wt% Ni_2P/MCM-41 is 83% and 84% for the DR method and TPR method, respectively. Interestingly, the best catalyst was prepared from the precursors with mole ratios (Ni/P) of 10/5 and 10/8 for the DR method and TPR method, respectively. Comparing the result in Fig. 13 and the results in Figs. 3b and 9, we see that the best synthesis conditions for the bulk and supported Ni_2P are

Table 3
The physical properties and HDS catalytic activities of the 10 wt% Ni_2P/MCM-41 catalysts prepared by different methods (testing conditions: 3 MPa, 310 °C, WHSV = 6 h^{-1}, H_2/oil = 720).

Catalysts	BET area ($m^2\ g^{-1}$)	CO uptake ($\mu mol\ g^{-1}$)	Conversion (%)	Selectivity (%)			TOF ($10^{-3}\ s^{-1}$)
				BP	BCH	CHB	
Ni_2P/MCM-41 (DR 10/5)	621	20	83	85.2	7.5	7.3	1.13
Ni_2P/MCM-41 (TPR 10/5)	616	20	73	85.3	7.6	7.1	0.99
Ni_2P/MCM-41 (TPR 10/8)	615	20	84	85.6	7.4	7.0	1.14

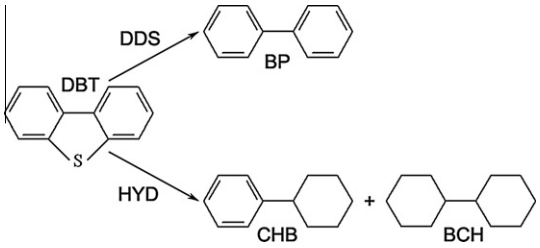

Scheme 1. Reaction pathway of the HDS of DBT on nickel phosphide catalysts.

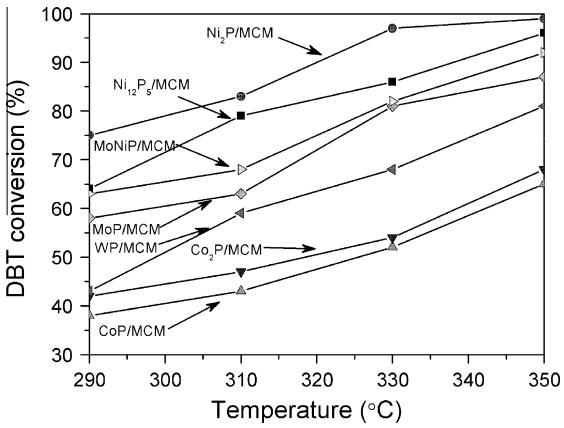

Fig. 14. The HDS catalytic activities of different catalysts (testing conditions: 3 MPa, WHSV = 6 h^{-1}, H_2/oil = 720).

identical. As shown in Fig. 9, bulk $Ni_{12}P_5$ and Ni_2P were obtained from the precursor with a mole ratio (Ni/P) of 10/5, and bulk Ni_2P was obtained from the precursor with a mole ratio (Ni/P) of 10/8. Wang et al. [20] also reported similar results: that temperature-programmed reduction of the precursor with Ni/P = 10/5 yielded $Ni_{12}P_5$/MCM-41, whereas reduction of the precursor with Ni/P = 10/8 produced Ni_2P/MCM-41. The HDS activity of Ni_2P is much higher than that of $Ni_{12}P_5$. Hence, the catalyst prepared using the TPR method from the precursor with a mole ratio (Ni/P) of 10/8 shows much better performance than that with a mole ratio (Ni/P) of 10/5.

For comparison, the physical properties and HDS catalytic activities of the 10 wt% Ni_2P/MCM-41 catalysts prepared by different methods are given in Table 3. It is seen that the catalyst prepared using the TPR method from the precursor with a mole ratio (Ni/P) of 10/8 shows physical properties and HDS catalytic activity similar to those of the catalyst prepared using the DR method from the precursor with a mole ratio (Ni/P) of 10/5, which indicates that the DR method also shows excellent performance in the synthesis of catalysts. Scheme 1 shows the reaction pathway for the HDS of DBT on nickel phosphide catalysts. It mainly involves hydrogenation (HYD) and direct desulfurization (DDS) pathways. The products of DBT HDS are mainly cyclohexylbenzene (CHB), bicyclohexane (BCH), and biphenyl (BP) [6,25]. The high BP selectivity (>85%) indicates that the DDS pathway is favored for DBT HDS over MCM-41-supported nickel phosphide catalysts.

In addition, different metal phosphides supported on MCM-41 containing 10 wt% of metal were synthesized and denoted as $Ni_{12}P_5$/MCM, Ni_2P/MCM, CoP/MCM, Co_2P/MCM, MoP/MCM, WP/MCM, and MoNiP/MCM. The detailed synthesis conditions for MCM-41-supported metal phosphides were the same as those for the bulk metal phosphides. Fig. 14 shows the HDS catalytic activities of different catalysts. The activities of all MCM-41-supported metal phosphide catalysts increased with increasing reaction temperature. The result indicates that the activities of the catalysts followed the order Ni_2P/MCM > $Ni_{12}P_5$/MCM > MoNiP/MCM > MoP/MCM > WP/MCM > Co_2P/MCM > CoP/MCM.

4. Conclusions

In summary, bulk and supported nickel phosphides were synthesized from phosphate precursors using the DR method. The new approach requires a low H_2 flow speed and is not affected by the heating rate. The results indicate that Ni_2P can be synthesized at 600 °C from the oxide precursors with a mole ratio of Ni/P = 2/1, and the synthesis conditions (e.g., loadings and H_2 flow speed) were also very broad. The preheating hydrogen, mole ratio of Ni/P, calcination temperature, and calcination time are all important factors in the DR method. The experimental results definitely indicate that the DR method is simple and feasible, providing an alternative way to synthesize nickel phosphides. The HDS activity results indicate that the DR method also shows excellent performance in the synthesis of catalysts. The high BP selectivity indicates that the DDS pathway is favored for DBT HDS over MCM-41-supported nickel phosphide catalysts.

Acknowledgments

This work was financially supported by the National NSFC (Grant 21073098), the Natural Science Foundation of Tianjin (11JCZDJC21600), the Research Fund for 111 Project (B12015), the Doctoral Program of Higher Education (20090031110015), and the Program for New Century Excellent Talents in University (NCET-10-0481).

Appendix A. Supplementary material

Supplementary data associated with this article can be found, in the online version, at http://dx.doi.org/10.1016/j.jcat.2012.11.008.

References

[1] S.T. Oyama, J. Catal. 216 (2003) 343.
[2] G. Li, F. Wang, Q. Jiang, X. Gao, P. Shen, Angew. Chem. Int. Ed. 49 (2010) 3653.
[3] K.L. Stamm, J.C. Garno, G. Liu, S.L. Brock, J. Am. Chem. Soc. 125 (2003) 4038.
[4] C.M. Grieb, R.H. Jones, J. Chem. Soc. (1932) 2543.
[5] X. Wang, P. Clark, S.T. Oyama, J. Catal. 208 (2002) 321.
[6] J.A. Cecilia, A. Infantes-Molina, E. Rodríguez-Castellón, A. Jiménez-López, J. Catal. 263 (2009) 4.
[7] Y. Xie, H.L. Su, X.F. Qian, X.M. Liu, Y.T. Qian, J. Solid State Chem. 149 (2000) 88.
[8] S. Yang, C. Liang, R. Prins, J. Catal. 237 (2006) 118.

[9] C. Qian, F. Kim, L. Ma, F. Tsui, P. Yang, J. Liu, J. Am. Chem. Soc. 126 (2004) 1195.
[10] A.E. Henkes, Y. Vasquez, R.E. Schaak, J. Am. Chem. Soc. 129 (2007) 1896.
[11] W.R. Robinson, G.J. van, T.I. Kor, S. Eijsbouts, K.A. van, V.J. van, B.V. de, J. Catal. 161 (1996) 539.
[12] A. Wang, M. Qin, J. Guan, L. Wang, H. Guo, X. Li, Y. Wang, R. Prins, Y. Hu, Angew. Chem. Int. Ed. 47 (2008) 6052.
[13] Q. Guan, W. Li, M. Zhang, K. Tao, J. Catal. 263 (2009) 1.
[14] Q. Guan, W. Li, J. Catal. 271 (2010) 413.
[15] J. Gopalakrishnan, S. Pandey, K. Kasthuri Rangan, Chem. Mater. 9 (1997) 2113.
[16] V.T. Silva, L.A. Sousa, R.M. Amorim, L. Andrini, S.J.A. Figueroa, F.G. Requejo, F.C. Vicentini, J. Catal. 279 (2011) 88.
[17] K. Cho, H. Seo, Y. Lee, Catal. Commun. 12 (2011) 470.
[18] G. Shi, J. Shen, J. Mater. Chem. 19 (2009) 2295.
[19] V. Zuzaniuk, R. Prins, J. Catal. 219 (2003) 85.
[20] A. Wang, L. Ruan, Y. Teng, X. Li, M. Lu, J. Ren, Y. Wang, Y. Hu, J. Catal. 229 (2005) 314.
[21] D. Fuks, D. Vingurt, M.V. Landau, M. Herskowitz, J. Phys. Chem. C 114 (2010) 13313.
[22] E. Larsson, Ark. Kem. 23 (1965) 335.
[23] Y.-K. Lee, S.T. Oyama, J. Catal. 239 (2006) 376.
[24] S.T. Oyama, X. Wang, Y.-K. Lee, W.-J. Chun, J. Catal. 221 (2004) 263.
[25] Q. Guan, C. Sun, R. Li, W. Li, Catal. Commun. 14 (2011) 114.